Trap-State-Induced Becquerel Type of Photoluminescence Decay in DPA-Activated Silicon Nanocrystals

Trap-state-induced Becquerel type of photoluminescence decay in DPA-activated silicon nanocrystals

K. Kůsová,[*,†] T. Popelář,[†] I. Pelant,[†] G. Morselli,[‡] S. Angeloni,[‡] and P. Ceroni[‡]

†*Institute of Physics of the ASCR, v.v.i., Cukrovarnická 10, 162 00 Prague 6, Czech Republic*
‡ *Chemistry Department "Giacomo Ciamician", University of Bologna, 40129 Bologna, Italy*

E-mail: kusova@fzu.cz

Abstract

A suitable description of the photoluminescence dynamics in a complex system such as an ensemble of semiconductor nanocrystals can bring invaluable insight into its carrier dynamics. In this contribution, we study a system of silicon nanocrystals sensitized by light-harvesting diphenylanthracene molecules enhancing their absorption. The emission-wavelength-resolved photoluminescence decay of this system can be well-described by the Becquerel (compressed-hyperbola) function, featuring a characteristic long tail. This shape of the photoluminescence decay function is linked to a model based on trapping and releasing of excited carriers, which are the cause of the long tail. Our model allows us to estimate the value of the trap capture cross-section of $\sigma_t \approx 1.5 \times 10^{-16}$ cm^2.

1 Introduction

Light-emitting nanoparticles, and in particular nanoparticles based on non-toxic and abundant materials, are potentially interesting for a wide range of applications, such as optoelectronics, sensing, imaging, photovoltaics or theranostics.[1,2] The understanding of luminescence decay kinetics and thus relaxation processes in nanoparticles is of utmost importance for their characterization and development of synthetic procedures. Many aspects of luminescence of nanoparticles can be characterized even on the single-nanocrystal level,[3] however, the more application-relevant study of the luminescence properties of ensembles of nanoparticles adds some additional parameters possibly influencing the decay kinetics of the sample to the "pure" physical model of a single emitting nanoparticle. These parameters and processes include for example the variations of size, shape or light-emission efficiency in the individual nanoparticles, the presence of traps or quenchers, or a possible interaction between the nanoparticles including various types of excitation transfer processes.

In an ideal-case scenario, the photoluminescence (PL) decay should follow a simple single-exponential law. This situation applies for example to dilute organic dyes[4,5] and a mono-exponential character has been observed experimentally in also single semiconductor nanostructures.[6,7] However, other experiments based on sophisticated time-tagged time-resolved single-photon counting techniques prove that the PL dynamics does not necessarily needs to be single-exponential even in single direct-bandgap NCs.[8] These results indicate that more than a single process can be responsible for the light emission even in a single nanoparticle, which can, in principle, be explained also simply by the thermal population of states.[9] Thus, not surprisingly, non-single-exponential PL dynamics are often observed even in systems of well-defined direct semiconductor NCs, especially in their densely-packed systems, as thoroughly described in Ref. (10) and references therein.

Ensembles of indirect-bandgap NCs are even more complicated in this context, because their decay lifetime τ is inherently dependent on the size of the nanoparticle, which inevitably causes a variation of light-emission-related properties in a sample. The distribution of sizes in such samples can be relatively broad.[11] The non-single-exponential kinetics[12,13] often appears even in emission-wavelength-resolved measurements, where the contributions of different sizes of NC should be limited. The measured PL decays are often approximated using the stretched-exponential (SE) law,[14] as probed by countless experiments, starting from porous-silicon-derived SiNCs in the 1990s[15–19] through SiNCs prepared by high-temperature annealing of Si-rich SiO_2 layers[20,21] to colloidal dodecene-capped SiNCs in the 2010s.[22–24] The SE dynamics appeared even at low temperatures[25] or in size-separated colloidal ensembles.[24]

Even though the observation of SE dynamics does not necessarily imply that a certain physical process is responsible for the observed shape of PL dynamics, several quantitative models leading to an SE decay shape were proposed, including a variation in lifetime from one NC to another,[12] the migration of exci-

tons between individual NCs,[25] or the above mentioned more recent homogeneous linewidth broadening.[22] However, even in an absence of a concrete model, the SE description can still be used as a simple measure of a deviation from a basic mono-exponential model.[26]

In this contribution, we show that the emission-wavelength-resolved PL dynamics of SiNCs follows a characteristic SE shape, however, this shape changes when light-harvesting diphenylanthracene (DPA) molecules covalently attached to the surface of SiNCs actively participate in the light emission process. The shape of the PL decay of the DPA-activated SiNCs can be well-described using a Becquerel decay law, which is characterized by a slightly longer tail and slower decay than the SE function. Using older literature, we adopt a quantitative model explaining the characteristic long-tail shape of a Becquerel-type decay in terms of trapping and releasing of excited carriers. Thus, we propose that this model can be revived for the description of more complex systems involving trapping of carriers.

2 Experimental

In order to investigate the PL dynamics of SiNCs in detail, we choose samples prepared based on the protocols published elsewhere.[27] In brief, SiNCs were synthesized by the thermal disproportionation of hydrogen silsequioxane and HF-etched, yielding free-standing H-terminated Si nanocrystals. These were then (i) alkyl-capped by hydrosilylation in the presence of 1-dodecene and initiated with diazonium salt and (ii) covalently functionalized with 9,10-diphenylanthracene chromophores using a two-step procedure. The diameter of the investigated SiNCs is about 4 nm.

Whereas the dodecene capped SiNC are well-known to exhibit PL characteristic of the quantum-confined core,[28] the mechanism of the cooperation between the SiNC and the DPA molecules on its surface is much less clear. Therefore, the PL of both these samples was thoroughly characterized using a system based on a fs laser Pharos with 150 fs pulses coupled to an optical parametric amplifier to change its wavelength to the visible range as the excitation source and a Hamamatsu streak camera coupled to an imaging spectrograph as the detection for time-resolved measurements. All the samples were colloidal dispersions of SiNCs in toluene stirred in a cuvette during the measurement and the detection was perpendicular to the excitation. All measurements were carried out at room temperature.

A dedicated analysis was applied to the measured data to maximize the extracted information.[30] This analysis is based on characterizing the measured PL decays $I(\lambda, t)$ at multiple wavelengths throughout the whole measured spectral range and at the same time taking into account the onset of PL (fitting a convolution of the decay function and a known Gaussian describing the laser pulse). Furthermore, the PL decays are measured using a relatively long temporal window (2 ms, i.e. using the 0.5 kHz repetition rate) to make sure that also the necessary tail of the PL decay is characterized with sufficient precision.[30]

3 Results and Discussion

3.1 Photoluminescence dynamics: stretched-exponential versus Becquerel decay

The measured data were fitted using four different functions to find out which model describes the type of wavelength-resolved PL decay the best. Their definitions and properties are compared in Fig. 1. In addition to the traditionally used single and stretched-exponential (SE) functions, we chose to include also a less well-known Becquerel (Bec, or "compressed-hyperbola") function[26,31] and a double exponential in the comparison of decay types.

Choosing a best model describing the observed behavior involves the comparison of goodness-of-fit statistics as shown in Fig. 2. Even though the single-number goodness-of-fit measures such as the number-of-free-parameters adjusted R^2 are minute, the shape of the best-fitting model can still be deter-

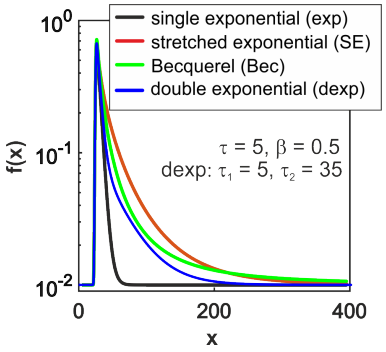

	$f(x)$	$\int_0^\infty f(x)\mathrm{d}x$	τ_{av}
$\exp(x;A,\tau)$	$A\exp\left\{-\frac{x}{\tau}\right\}$	τ	τ
$\mathrm{SE}(x;A,\tau,\beta)$ [14,29]	$A\exp\left\{-\left(\frac{x}{\tau}\right)^{\beta}\right\}$	$\frac{\tau}{\beta}\Gamma\left(\frac{1}{\beta}\right)$	$\frac{\Gamma(2/\beta)}{\Gamma(1/\beta)}\tau$
$\mathrm{Bec}(x;\tau,\beta)$ [26]	$A/\left[1+(1-\beta)\frac{x}{\tau}\right]^{\frac{1}{1-\beta}}$	$\frac{\tau}{\beta}$	$\frac{\tau}{2\beta-1}$, $\beta>0.5$
$\mathrm{dexp}(x;A_1,A_2,\tau_1,\tau_2)$	$\sum_{i=1}^{2}A_i\exp\left\{-\frac{x}{\tau_i}\right\}$	$\tau_1+\tau_2$	$\frac{\tau_1+\tau_2}{2}$

Figure 1: Overview of the discussed functions. The figure shows a comparison of the discussed functions plotted in the offset logarithmic scale.[30] The table on the right presents a summary of selected important properties of these functions. The β parameter is from the interval $0<\beta\leq 1$ for both the stretched exponential and the Bec functions and both these functions become a single exponential in the limiting case where $\beta=1$. $\Gamma()$ is the standard gamma function. The integral is shown for $A=1$. The average lifetime τ_{av} is the ("intensity") average lifetime $\tau_{\mathrm{av}}=\frac{\int_0^\infty xf(x)\mathrm{d}x}{\int_0^\infty f(x)\mathrm{d}x}$, which, from the physical point of view, corresponds to the average time during which the emitters remain in the excited state after the end of an excitation pulse.[14] See the Supporting Information for the formulas of the corresponding errors.

mined using more specialized statistical tools. In this regard, the autocorrelation function of weighted residuals (ACF) can be viewed as the most useful tool.[31] As the residuals measure the absolute deviation of the data from the fit, they should be weighted by the square root of the fitting function to represent the relative rather than absolute deviation.[31] Moreover, ACF can be applied to quantities investigated as functions of a single parameter such as the fluctuations in the emitted intensity in time to characterize a signal possessing a degree of randomness,[32–34] or it can be calculated for three-dimensional dependencies ("maps")[35,36] such as the residuals studied here. The ACF of weighted (normalized) residuals is thus calculated as

$$\begin{aligned}&\mathrm{ACF}(\Delta t,\Delta\lambda)=\\&=\mathrm{iFFT}\left\{\mathrm{FFT}\left(\frac{I(\lambda,t)-f(\lambda,t)}{\sqrt{f(\lambda,t)}}\right)\cdots\right.\\&\left.\cdots\,\mathrm{FFT}^{*}\left(\frac{I(\lambda,t)-f(\lambda,t)}{\sqrt{f(\lambda,t)}}\right)\right\},\end{aligned}\tag{1}$$

where (i)FFT stands for the (inverse) Fourier transform, * is the complex conjugate, I are the measured data and f is the fitted function calculated in the same points (λ,t) at which the data were measured.

In general, ACF can help reveal difficult-to-find dependencies in noisy data, because noise does not correlate. Therefore, in a three-dimensional case, an ACF of only noise, characterizing a good fit, would be a "map" with a single larger value in the center $(\Delta\lambda,\Delta t)=0$, corresponding to the correlation of one point with itself, whereas the rest of the ACF data should be featureless, randomly distributed around a single value (forming a "plane"). However, if non-random trends are present in the data, corresponding to a worse fit in the case of residuals, a trend would be visible in the off-center part of the ACF.

The ACF's of weighted residuals from Eq. (1) for the fits of PL decays measured in the SiNC and the activated SiNC sample assuming the four fitting functions from Fig. 1 are presented in Fig. 2. Clearly, in both cases, a single exponential is not a good fit because the ACF is strongly non-planar, while the double exponential's residuals are featureless, signifying a perfect fit. The differences between the SE and Bec fits are relatively small, but the projections of the logarithmically plotted ACF to the $(\Delta t,\Delta\lambda)$ plane shown at the bottom of the ACF plots in Fig. 2 exhibit smaller deviations from the ideal

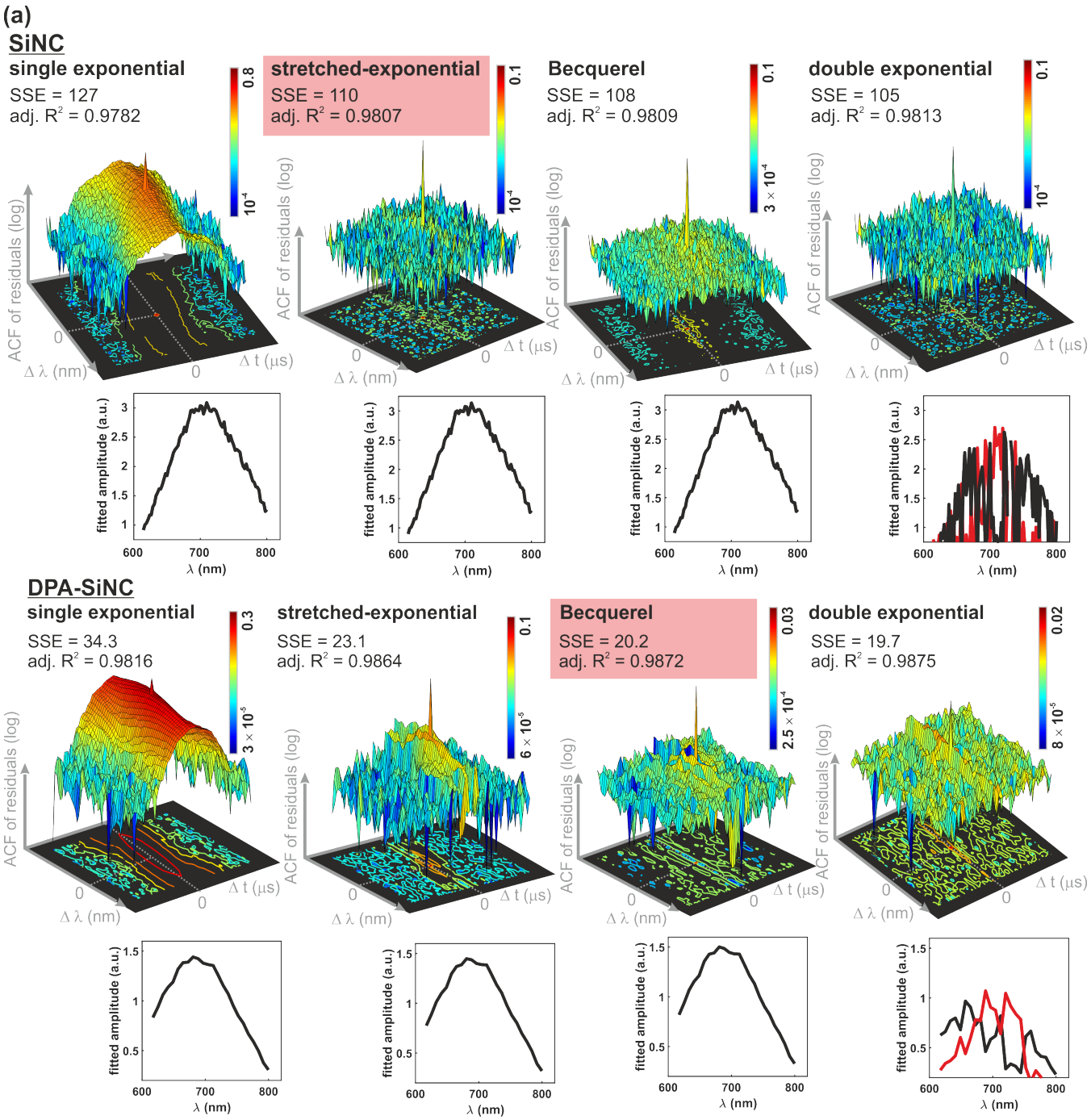

Figure 2: The comparison of fits using different fitting models from Fig. 1 for the two investigated samples: ordinary SiNC (a) and DPA-activated SiNC (b). Each panel presents the autocorrelation function of weighted residuals plotted from Eq. (1) in logarithmic scale for the four considered functions at the top and a plot of fitted amplitudes A at the bottom. The ACF was resampled (linearly interpolated) to the size of 75×75 points^2 for the purposes of the visual presentation except for the center point, whose value was kept. The projection of the logarithmic ACF plot to the $(\Delta t, \Delta\lambda)$ plane, which better highlights possible deviations from a planar shape, is shown below each ACF plot. Additionally, the sum of squares due to error (SSE) and the the R-square adjusted for the number of free parameters (adj. R^2) are also listed. The best-fit functions are highlighted by the red rectangles.

planar shape based on the SE and Bec fits for the sample of SiNCs and activated SiNCs, respectively, indicating the two different fitting functions for the two samples. If the choice now is between a double exponential and a streched-exponential (or Bec) type of PL decay for the SiNC (or the activated SiNC) sample, respectively, we need to note that a double exponential curve has one more free parameter (the total of four) when compared to the two latter functions (a total of three). Whereas the fitted amplitudes shown in Fig. 2 for the exponential, SE and Bec types of decay simply copy the measured spectrum, the two amplitudes of the double-exponential decay curve produce a noisy spectrum, implying an over-parametrized function. Therefore, a SE and a Bec type of PL decay were chosen to best describe the measured PL intensities of the SiNC and activated SiNC sample, respectively, and are used in the following text.

These fit comparison results can be summed in two important points: (i) the SE and Bec PL decay curves describe the shape of the wavelength-resolved PL decay in SiNCs very well and (ii) the SE shape of the PL decay can change to a different one (in our case from SE to Bec), implying that the shape of the PL decay curve still carries some information about the processes responsible for the emission of light.

The PL decay characteristics were then investigated for different excitation intensities in the two samples in question. During the fitting, no clear dependence for the β parameters was observed throughout the investigated spectral region, and therefore the $\beta(\lambda)$ values were fixed at the weighted mean for each excitation intensity. The SE β parameters of the SiNC sample show a slight increase with increasing excitation intensity from 0.81 to 0.85, whereas the Bec β parameters characterizing the DPA-SiNC sample are around 0.73 for in the whole range of investigated excitation intensities (not shown). The results of the analysis are summarized in Fig. 3(b,c), which presents the fitted (intensity) averaged lifetimes τ_{av} calculated from the $\tau(\lambda)$ and β fit parameters using the formulas shown in the table in Fig. 1. The average lifetimes are chosen because they provide a better comparison between the individual measurements (especially when the fitting functions are different) than simply using the fitted τ.[13,14] The average lifetimes are, within the experimental error, the same for all the investigated excitation intensities and they very well follow a single-exponential trend with emission wavelengths. The single-exponential trend of the average lifetimes as a function of emission wavelength (i.e. NC sizes) is a consequence of the quantum-confined origin of the emitted PL and the indirect nature of the bandgap of these SiNCs.[12] Interestingly, a similar, also single-exponential curve was predicted theoretically using tight-binding calculations of SiNCs of various sizes in an SiO_2 matrix including both no-phonon and phonon-assisted processes.[12] Compared to those calculations, the measured $\tau_{\mathrm{av}}(\lambda)$ dependence in our study has about $4\times$ larger pre-factor ($75\ \mathrm{s}^{-1}$ vs. $20\ \mathrm{s}^{-1}$) and basically the same decay constant (0.35 eV vs. 0.31 eV). The difference in the pre-factor, causing shorter decay lifetimes (faster rates) in our samples, can be caused by the influence of the SiO_2 matrix in the calculations, or by the short-pulse excitation, which yields shorter measured lifetimes.[13] Remarkably, the decay constants of the dependence are the same as in the calculations, implying that the effect of quantum confinement is the same as predicted.

Despite the attachment of the DPA molecules to the DPA-SiNC sample, the evolution of the average lifetimes with emission wavelength is remarkably similar and it keeps the single-exponential dependence, except for being somewhat shifted towards shorter lifetime values. This similarity strongly suggests that the observed PL is of the same origin in the two samples and that the attachment of the DPA molecules only slightly modifies the underlying processes.

The fitted amplitudes of the $A(\lambda)$ of the PL decay measurements then constitute the PL spectra and are shown in Fig. 3(d). Clearly, the changes with excitation intensity are only minor in both the sample and the most important difference is a small blueshift by about 20 nm between the SiNC ($\mathrm{PL}_{\mathrm{max}}$ at 740 nm) and the DPA-SiNC ($\mathrm{PL}_{\mathrm{max}}$ at 720 nm) sample.

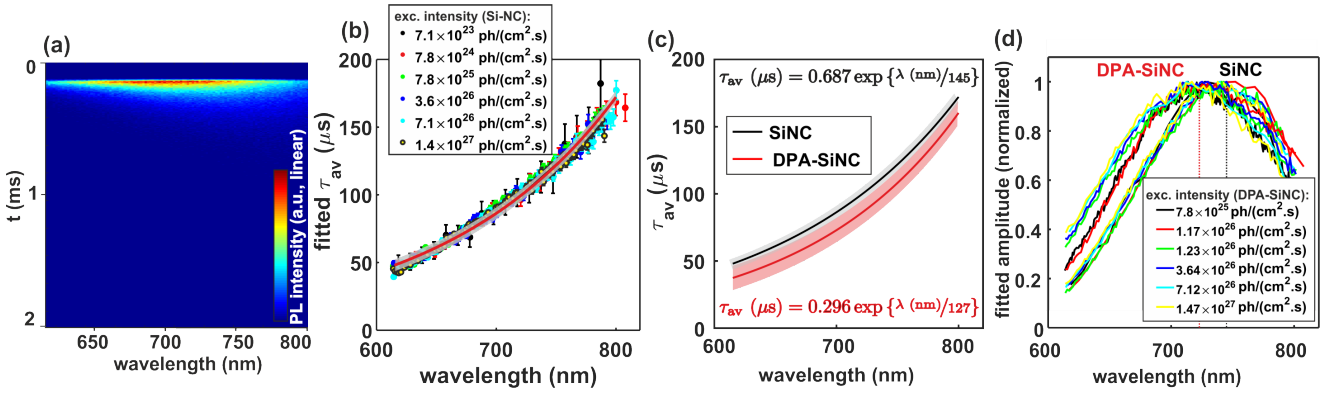

Figure 3: The measured excitation-intensity dependence of the PL characteristics of the samples using a 400-nm excitation wavelength. (a) An example of the measured PL intensity dependence. (b) Average lifetimes calculated based on table in Fig. 1 (the gray area highlights the 95 % confidence bands) from a series of measurements carried out at different excitation intensities on the SiNC sample. The fit assumes an exponential dependence on the emission wavelengths λ. (c) The fit of average lifetimes for the SiNC sample redrawn from panel (b) to be compared to the same dependence for the DPA-SiNC sample. The fitted formulas are included in the figure. The fit for the SiNC sample in the photon energy units reads: $1/\tau_{\mathrm{av}\,(\mu\mathrm{s})} = 76.2 \exp\{E_{\mathrm{ph}\,(\mathrm{eV})}/0.354\}$. No clear dependence was observed in the β parameters from the table in Fig. 1. (d) The corresponding normalized fitted amplitudes (PL spectra). The excitation-intensity legend for the SiNC sample is the same as in panel (b).

In addition to the excitation-intensity dependence, also the effect of excitation wavelength was investigated in the DPA-activated SiNC sample in the excitation spectral range of $315 - 480$ nm. As shown in Fig. 4(a), the DPA molecules have the strongest absorption around 400 nm, which is a spectral range where the attachment of the DPA molecules to the surface of SiNCs should have the highest impact on the properties of the NC. The absorption spectrum of the DPA-activated SiNCs (the green curve in Fig. 4(a)) is clearly a superposition of the absorption spectra of the dodecene-capped SiNCs and the DPA molecules, confirming that the attachment of the DPA molecules boosts the absorption of the SiNCs.

A change in the character of the PL decay was observed within the investigated excitation-wavelength range, see Fig. 4(a). Whereas close to the "resonant" excitation wavelength of 400 nm, the observed PL decay follows the Bec function, outside of this range the decay is more SE in nature, even though the SE description does not fit the data perfectly in this case. The quality of the description of the PL decays using the two function can again be judged using the ACF formalism as shown in Fig. 4(b,c). Firstly, both ACF's show a deviation from a noise signal around $\Delta t = 0$ µs throughout the whole emission wavelength range. This deviation suggests a discrepancy between the data and the function used for their description around the beginning of the PL decay, pointing towards the presence of a shorter component in the decay (or possibly jitter of the excitation laser). Secondly, unlike in the case of SiNCs in Fig. 2, the SE fit of the DPA-SiNC sample outside the "resonant" excitation-wavelength range in Fig. 4(b) shows some deviation also in the tail of the PL decay. This deviation implies that even though the PL decay is more SiNC-like, the mechanism causing the Bec type of PL decay is still present. Thus, in order to describe this cooperation of two types of mechanisms better, a more elaborate model than the one we are currently applying would be necessary. However, since the deviation is very small, the description of the measured data using the SE function is still a very good approximation of the real behavior. Interestingly, the change of the character of PL decay is accompanied by changes in PL spectra, where the spectrum slightly blueshifts in the

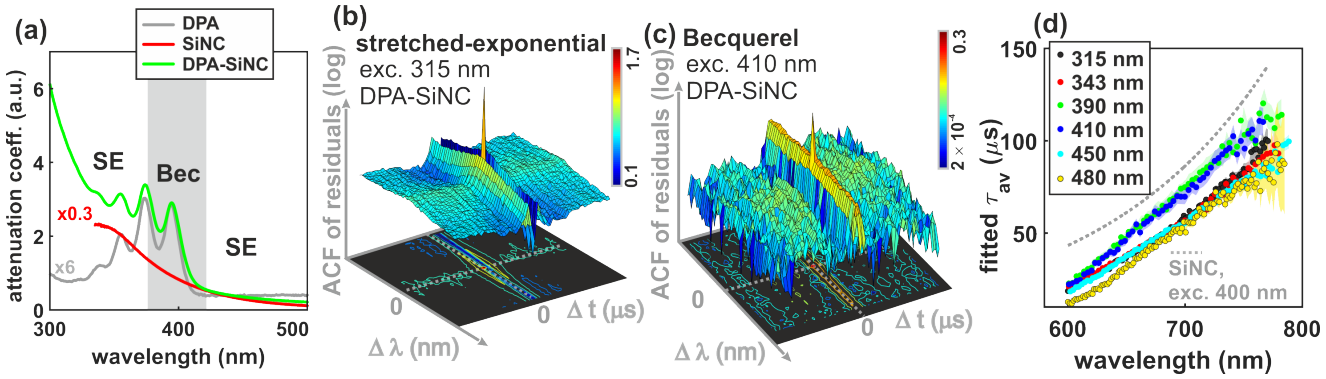

Figure 4: PL decay as a function of excitation wavelength for the DPA-SiNC sample. (a) Absorbance spectrum. The absorbance curves of some of the samples were rescaled to make the comparison of the shapes easier. The gray area designates the excitation spectral range leading to the Becquerel type of PL decay, outside this range the PL decay has a more SE character. Autocorrelation of weighted residuals of (b) an SE and (c) a Becquerel-based fit under (b) 315 nm and (c) 410 nm excitation, respectively. (d) The excitation-wavelength dependence of the fitted average lifetimes, the dotted gray curve is redrawn from Fig. 3(b). All indicated errors are 95% confidence (prediction) bands.

Bec regime and redshifts in the SE regime (not shown), implying changes analogical to those in Fig. 3(d).

As regards the average lifetimes, they again rise single-exponentially with increasing emission wavelength and are very close to those in SiNCs, see Fig. 4(d). In agreement with Fig. 3(c), the average lifetimes are only slightly shorter than those in SiNCs inside the DPA-boosted excitation-wavelength range. Outside of this range, they further fall to values about 2× shorter than those in SiNCs. Since this drop is more or less the same throughout the whole emission-wavelength range, it is likely that the drop in the average lifetimes is caused by the overall increase of the importance of fast-decaying non-radiative channels (the measured lifetime τ is influenced by both the radiative τ_{rad} and non-radiative $\tau_{\mathrm{non-rad}}$ lifetimes $1/\tau = \sum_i 1/\tau_{\mathrm{rad}}^{(i)} + \sum_i 1/\tau_{\mathrm{non-rad}}^{(i)}$, where i indexes the recombination channels).

3.2 Microscopic model

The above findings imply that the character of the emission-wavelength-resolved PL decay of SiNC changes from SE to Bec-like when DPA molecules covalently attached to the surface of SiNCs actively take part in the excitation-recombination process. The possible mechanisms responsible for the SE character have been already proposed,[12,22,25] however, the Bec function is much less well-known.

The Bec decay law in the form presented in the table in Fig. 1 is generally speaking a solution to a kinetic equation of the type[26]

$$\frac{\mathrm{d}N}{\mathrm{d}t} = -kN^{2-\beta}, \quad 0 \leq \beta \leq 1 \qquad (2)$$

where N is the concentration of luminescence centers and the emitted PL intensity $I(t) = I_0 N(t)$. It was used in the past to describe the PL decay of crystalline phospors.[37] More recently, it has been shown to result also from a gamma-distributed fluctuations of lifetimes and experimentally confirmed in the fluorescence of complex molecules.[38] For a limiting case of $\beta \to 1$ the Bec model reduces to a simple single-exponential[26] and for $\beta \to 0$ the decay law has the form of a hyperbola (a power law).

As long time ago as in the middle of the last century, Adirovitch[37] and Fok[39] developed a model describing a crystalline phospor where the excited carriers were trapped from conduction band and consequently released back and in which the PL decay follows the Bec law. This model is derived for a special case of $\beta = 1/2$, however, the author generalizes the model by

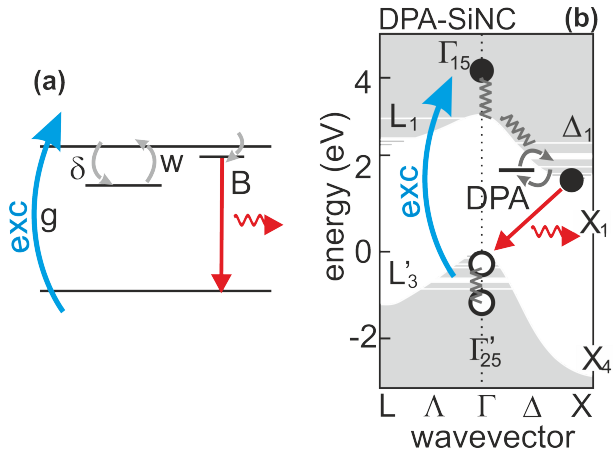

Figure 5: (a) Real-space sketch of a model leading to a Bec type of PL decay. (b) The same model shown for DPA-activated SiNCs, where the relaxation processes in SiNCs are approximated using the bandstructure concept.

saying that the experimentally observed values of the β coefficient can be in a broader interval. Thus, it can be applied also to our situation at least to make an order-of-magnitude estimate, since the difference in the β parameters is small ($\beta = 0.73$ in our measurements).

Thus, this model should be of interest also now and can be revived for the description of the PL of more complex systems involving trapping of carriers. The model is based on a system of kinetic equations describing the process sketched in Fig. 5(a), where the re-trapping and releasing of excited carriers to the conduction band causes the long tail of the Bec type of PL decay. In particular, the authors[37,39] show that observed PL can be written in the form

$$I(t) = \frac{1}{(1+Kt)^2}, \quad K = \sqrt{\frac{gwB}{\delta}}, \qquad (3)$$

where $g(^1/_{\mathrm{cm^3 s}})$ is the rate of the photoexcitation of carriers, $w(\mathrm{s}^{-1})$ is the probability of the electron escaping the trap, $B(^{\mathrm{cm}^3}/_{\mathrm{s}})$ is the radiative recombination coefficient and $\delta(\mathrm{s}^{-1})$ is the electron trapping rate (see Fig. 5(a)). This rate is given by the trap capture cross-section σ_t, the thermal velocity of an electron v_{th} and the overall concentration of traps n_t as $\delta = \sigma_t v_{\mathrm{th}} n_t$. This theoretically predicted decay law can be combined with the measured PL decay $K \approx {}^1/_{2\tau}$, which allows for the determination of the capture cross-section from the measured decay τ

$$\sigma_t = \frac{4\tau^2 gwB}{v_{\mathrm{th}} n_t}. \qquad (4)$$

This trapping model can be applied to the PL of the DPA-SiNC sample since the attachment of the DPA molecules can be expected to lead to the formation of DPA-related trap states in the NC, see Fig. 5(b). This trap state could be connected with the lowest excited DPA level, which is a triplet state and is energetically close to the observed emission (1.77 eV→ 700 nm).[40] First of all, the known molar extinction coefficient $\varepsilon = 1.5 \times 10^5\ \mathrm{M}^{-1}\mathrm{cm}^{-1}$ (at 430 nm[27]) can be recalculated to the absorption cross-section $\sigma_{\mathrm{NC}} = {}^{1000\varepsilon}/_{N_A} = 2.5 \times 10^{-16}\ \mathrm{cm}^2$. Moreover, using the attenuation coefficient $\alpha = 2\ \mathrm{cm}^{-1}$ determined from the transmission of the SiNC sample T along an optical path l

$$\alpha = -{}^{\ln(T)}/_l = \sigma_{\mathrm{NC}} c_{\mathrm{NC}}, \qquad (5)$$

we can easily calculate the concentration of NCs in the sample as $c_{\mathrm{NC}} = {}^{\alpha}/_{\sigma_{\mathrm{NC}}} = 8 \times 10^{15}\ {}^{\mathrm{NC}}/_{\mathrm{cm}^3}$. Next, the radiative recombination coefficient can be obtained from the radiative lifetime of SiNCs (assuming a 25 % PL quantum yield QY) $\tau_{\mathrm{rad}}^{\mathrm{SiNC}} = {}^{\tau_{\mathrm{av}}^{\mathrm{SiNC}}}/_{\mathrm{QY}} = 450\ \mu\mathrm{s}$ and the known concentration of NCs c_{NC} as $B = {}^1/_{(\tau_{\mathrm{rad}}^{\mathrm{SiNC}} c_{\mathrm{NC}})}$. The thermal velocity of an electron at room temperature is $v_{\mathrm{th}} = 10^7\ {}^{\mathrm{cm}}/_{\mathrm{s}}$. In order to determine the concentration of traps we can make

an estimate of about $N_{\mathrm{tr}} = 100$ traps per one NC (as estimated based on absorption spectra in Ref. (27)), thus $n_t \approx N_{\mathrm{tr}} c_{\mathrm{NC}}$. The probability of an electron escaping from the trap w is difficult to estimate, but it clearly needs to be of the order of the reciprocal radiative lifetimes, because otherwise the PL would be quickly quenched: $w \approx {}^{1}/_{\tau_{\mathrm{rad}}^{\mathrm{SiNC}}}$. The generation term g can be expressed as $g = \alpha\Phi$, where Φ is the impinging photon flux. Using these values, Eq. (4) reduces to

$$\sigma_t \approx \frac{4\left(\tau^{\mathrm{DPA-SiNC}}\right)^2}{\left(\tau_{\mathrm{rad}}^{\mathrm{SiNC}}\right)^2} \frac{\alpha\Phi}{N_{\mathrm{tr}} v_{\mathrm{th}} c_{\mathrm{NC}}^2} = \frac{4 \times 10^{-7}}{N_{\mathrm{tr}}} \left(\frac{\tau^{\mathrm{DPA-SiNC}}}{\tau_{\mathrm{rad}}^{\mathrm{SiNC}}}\right)^2 \frac{\sigma_{\mathrm{NC}}^2 \Phi}{\alpha}, \tag{6}$$

where the material constant of the absorption cross-section from Eq. (5) is used rather than the calculated (and relatively difficult to determine) NC concentration c_{NC}. Now, we can simply insert the known values into Eq. (4). In the above text, we showed that $\alpha = 2\ \mathrm{cm}^{-1}$ and $\Phi = 10^{26}\ {}^{\mathrm{photons}}/_{\mathrm{cm^2 s}}$. PL measurements from Fig. 3(c) give us the values of $\tau^{\mathrm{DPA-SiNC}} = 50\ \mu\mathrm{s}$. Thus, $\sigma_t \approx 1.5 \times 10^{-16}\ \mathrm{cm}^2$.

Adirovitch's model then allows one to determine also the value of the luminescence center capture cross-section σ_c for an electron released from the trap, through the experimentally observed β coefficient $\sigma_c = \frac{\sigma_t}{\gamma(\beta)}$. Following the argumentation provided in Ref. (37), we can make a rough (order-of-magnitude) estimate of the $\gamma(\beta)$ coefficient of ${}^{1}/_{10}$, which yields $\sigma_c \approx 10\sigma_t = 10^{-15}\ \mathrm{cm}^2$.

4 Conclusions

In conclusion, we show that the attachment of DPA molecules to the surface of Si nanocrystals changes the shape of their emission-wavelength-resolved photoluminescence decay curve from stretched-exponential to the Becquerel type in the excitation-wavelength region in which the DPA molecules influence the excitation process the most. A microscopic model based on the trapping and release of excited carriers is used to estimate the trap and center capture cross-sections ($\sigma_t \approx 1.5 \times 10^{-16}\ \mathrm{cm}^2$, $\sigma_c \approx 10^{-15}\ \mathrm{cm}^2$), which is the process causing the characteristic long tail of the photoluminescence decay. The Becquerel-function shape of photoluminescence decay can be applied to other materials, in which relaxation processes involve the trapping of carriers.

Acknowledgement The Czech Science Foundation funding, Grant No. 18-05552S (KK, TP, IP), the Operational Programme Research, Development and Education financed by European Structural and Investment Funds and the Czech Ministry of Education, Youth and Sports (Project No. SOLID21 CZ.02.1.01/0.0/0.0/16_019/0000760, KK) are gratefully acknowledged.

Supporting Information Available

Supporting Information details formulas for the errors of the quantities from Table 1.

References

(1) Kovalenko, M. V.; Manna, L.; Cabot, A.; Hens, Z.; Talapin, D. V.; Kagan, C. R.; Klimov, V. I.; Rogach, A. L.; Reiss, P.; Milliron, D. J. et al. Prospects of Nanoscience with Nanocrystals. *ACS Nano* **2015**, *9*, 1012–1057.

(2) Mazzaro, R.; Romano, F.; Ceroni, P. Long-lived luminescence of silicon nanocrystals: from principles to applications. *Phys. Chem. Chem. Phys.* **2017**, *19*, 26507–26526.

(3) K. Kůsová, In *21st Century Nanoscience—A Handbook: Advanced Analytic Methods and Instrumentation (Volume 3)*; Sattler, K. D., Ed.; Taylor&Francis Publisher, CRC Press: Boca Raton, Florida, USA, 2020; pp 21(1)–(25).

(4) Boens, N.; Qin, W.; Basarić, N.; Hofkens, J.; Ameloot, M.; Pouget, J.; Lefèvre, J.-P.; Valeur, B.; Gratton, E.; vandeVen, M. et al. Fluorescence Lifetime Standards for Time and Frequency Domain Fluorescence Spectroscopy. *Anal. Chem.* **2007**, *79*, 2137–2149.

(5) Chung, P.-H.; Tregidgo, C.; Suhling, K. De-

termining a fluorophore's transition dipole moment from fluorescence lifetime measurements in solvents of varying refractive index. *Methods Appl. Fluoresc.* **2016**, *4*, 045001.

(6) Htoon, H.; Malko, A. V.; Bussian, D.; Vela, J.; Chen, Y.; Hollingsworth, J. A.; Klimov, V. I. Highly Emissive Multiexcitons in Steady-State Photoluminescence of Individual "Giant" CdSe/CdS Core/Shell Nanocrystals. *Nano Lett.* **2010**, *10*, 2401–2407.

(7) Amloy, S.; Moskalenko, E. S.; Eriksson, M.; Karlsson, K. F.; Chen, Y. T.; Chen, K. H.; Hsu, H. C.; Hsiao, C. L.; Chen, L. C.; Holtz, P. O. Dynamic characteristics of the exciton and the biexciton in a single InGaN quantum dot. *Appl. Phys. Lett.* **2012**, *101*, 061910.

(8) Galland, C.; Ghosh, Y.; Steinbrück, A.; Sykora, M.; Hollingsworth, J.; Klimov, V. I.; Htoon, H. Two types of luminescence blinking revealed by spectroelectrochemistry of single quantum dots. *Nature* **2011**, *479*, 203–207.

(9) Dohnalová, K.; Hapala, P.; K. Kůsová,; Infante, I. Band-gap and radiative rate tunability achieved via ligands in covalent, as opposed to ionic, semiconductor nanocrystal. *Chem. Mater.* **2020**, *32*, 6326–6337, journal cover, ACS AuthorChoice.

(10) Bodunov, E. N.; Simões Gamboa, A. L. Kinetics of Photoluminescence Decay of Colloidal Quantum Dots: Nonexponential Behavior and Detrapping of Charge Carriers. *J. Phys. Chem. C* **2018**, *122*, 10637–10642.

(11) Zajac, V.; Němec, H.; Kadlec, C.; K. Kůsová,; Pelant, I.; Kužel, P. THz photoconductivity in light-emitting surface-oxidized Si nanocrystals: the role of large particles. *New J. Phys.* **2014**, *16*, 093013.

(12) Delerue, C.; Allan, G.; Reynaud, C.; Guillois, O.; Ledoux, G.; Huisken, F. Multiexponential photoluminescence decay in indirect-gap semiconductor nanocrystals. *Phys. Rev. B* **2006**, *73*, 235318.

(13) Greben, M.; Valenta, J. Power-dependent photoluminescence decay kinetics of silicon nanocrystals under continuous and pulsed excitation. *Faraday Discuss.* **2020**, *222*, 274–293.

(14) Greben, M.; Khoroshyy, P.; Sychugov, I.; Valenta, J. Non-exponential decay kinetics: correct assessment and description illustrated by slow luminescence of Si nanostructures. *Appl. Spectrosc. Rev.* **2019**, *0*, 1–44.

(15) Vial, J. C.; A., B.; Gaspard, F.; Hérino, R.; Ligeon, M.; Muller, F.; Romestain, R.; Macfarlane, R. M. Mechanisms of visible-light emission from electro-oxidized porous silicon. *Phys. Rev. B* **1992**, *45*, 14171–14176.

(16) Chen, X.; Henderson, B.; ; O'Donnell, K. P. Luminescence decay in disordered low-dimensional semiconductors. *Appl. Phys. Lett.* **1992**, *60*, 2672–2674.

(17) Mihalcescu, I.; Vial, J. C.; Romestain, R. Carrier localization in porous silicon investigated by time-resolved luminescence analysis. *J. Appl. Phys.* **1996**, *80*, 2404.

(18) Pavesi, L.; Ceschini, M. Stretched-exponential decay of the luminescence in porous silicon. *Phys. Rev. B* **1993**, *48*, 17625–17628.

(19) Xie, Y. H.; Wilson, W. L.; Ross, F. M.; Mucha, J. A.; Fitzgerald, E. A.; Macaulay, J. M.; Harris, T. D. Luminescence and structural study of porous silicon films. *J. Appl. Phys.* **1992**, *71*, 2403–2407.

(20) Linnros, J.; Lalic, N.; Galeckas, A.; Grivickas, V. Analysis of the Stretched Exponential Photoluminescence Decay from Nanometer-sized Silicon Crystals in SiO_2. *J. Appl. Phys.* **1999**, *86*, 6128.

(21) Dunn, K.; Derr, J.; Johnston, T.; Chaker, M.; Rosei, F. Multiexponential photoluminescence decay of blinking nanocrystal ensembles. *Phys. Rev. B* **2009**, *80*, 035330.

(22) Sangghaleh, F.; Sychugov, I.; Yang, Z.; Veinot, J. G. C.; Linnros, J. Near-Unity Internal Quantum Efficiency of Luminescent Silicon Nanocrystals with Ligand Passivation. *ACS Nano* **2015**, *9*, 7097–7104.

(23) Greben, M.; Khoroshyy, P.; Liu, X.; Pi, X.; Valenta, J. Fully radiative relaxation of silicon nanocrystals in colloidal ensemble revealed by advanced treatment of decay kinetics. *J. Appl. Phys.* **2017**, *122*, 034304.

(24) Brown, S. L.; Krishnan, R.; Elbaradei, A.; Sivaguru, J.; Sibi, M. P.; Hobbie, E. K. Origin of stretched-exponential photoluminescence relaxation in size-separated silicon nanocrystals. *AIP Adv.* **2017**, *7*, 055314.

(25) Pavesi, L. Influence of dispersive exciton motion on the recombination dynamics in porous silicon. *J. Appl. Phys.* **1996**, *80*, 216–225.

(26) Berberan-Santos, M.; Bodunov, E.;

Valeur, B. Mathematical functions for the analysis of luminescence decays with underlying distributions: 2. Becquerel (compressed hyperbola) and related decay functions. *Chem. Phys.* **2005**, *317*, 57 – 62.

(27) Mazzaro, R.; Gradone, A.; Angeloni, S.; Morselli, G.; Cozzi, P. G.; Romano, F.; Vomiero, A.; Ceroni, P. Hybrid Silicon Nanocrystals for Color-Neutral and Transparent Luminescent Solar Concentrators. *ACS Photonics* **2019**, *6*, 2303–2311.

(28) Hannah, D. C.; Yang, J.; Podsiadlo, P.; Chan, M. K. Y.; Demortiére, A.; Gosztola, D. J.; Prakapenka, V. B.; Schatz, G. C.; Kortshagen, U.; Schaller, R. D. On the Origin of Photoluminescence in Silicon Nanocrystals: Pressure-Dependent Structural and Optical Studies. *Nano Lett.* **2012**, *12*, 4200–4205.

(29) Berberan-Santos, M.; Bodunov, E.; Valeur, B. Mathematical functions for the analysis of luminescence decays with underlying distributions 1. Kohlrausch decay function (stretched exponential). *Chem. Phys.* **2005**, *315*, 171 – 182.

(30) K. Kůsová,; Popelář, T. On the importance of onset times and multiple-wavelength analysis of photoluminescence decays. *J. Appl. Phys.* **2019**, *125*, 193103.

(31) Lemmetyinen, H.; Tkachenko, N. V.; Valeur, B.; Hotta, J.-i.; Ameloot, M.; Ernsting, N. P.; Gustavsson, T.; Boens, N. Time-resolved fluorescence methods (IUPAC Technical Report). *Pure Appl. Chem.* **2014**, *86*, 1969–1998.

(32) Verberk, R.; Orrit, M. Photon statistics in the fluorescence of single molecules and nanocrystals: Correlation functions versus distributions of on- and off-times. *J. Chem. Phys.* **2003**, *119*, 2214–2222.

(33) Bruhn, B.; Qejvanaj, F.; Gregorkiewicz, T.; Linnros, J. Temporal correlation of blinking events in CdSe/ZnS and Si/SiO_2 nanocrystals. *Phys. B Condens. Matter* **2014**, *453*, 63–67.

(34) K. Kůsová,; Pelant, I.; Humpolíčková, J.; Hof, M. Comprehensive description of blinking-dynamics regimes in single direct-band-gap silicon nanocrystals. *Phys. Rev. B* **2016**, *93*, 035412.

(35) Roger L. Easton, J. *Fourier Methods in Imaging*; Wiley, Chester F. Carlson Center for Imaging Science, Rochester NY, USA, 2010.

(36) Fekete, L.; K. Kůsová,; Petrák, V.; Kratochvílová, I. AFM topographies of densely packed nanoparticles: a quick way to determine the lateral size distribution by autocorrelation-function analysis. *J. Nanopart. Res.* **2012**, *14*, 1062.

(37) Adirovitch, E. La formule de Becquerel et la loi élémentaire du déclin de la luminescence des phosphores cristallins (The Becquerel formula and the basic law of the luminescence decay in crystalline phospors, in French). *J. Phys. Radium* **1956**, *17*, 705–707.

(38) Włodarczyk, J.; Kierdaszuk, B. Interpretation of fluorescence decays using a power-like model. *Biophys. J.* **2003**, *85*, 589–598.

(39) Fok, M. V. *Introduction to the kinetics of crystal luminescence (in Russian)*; Nauka, Moscow, Russia, 1964.

(40) Ting, C.-H. Electronic structure and intersystem crossing in 9,10-diphenylanthracene. *Chem. Phys. Lett.* **1967**, *1*, 335–336.